Equivalent: Jurnal Ilmiah Sosial Teknik
Volume 8, Issue 4, 1852-1871
e_ISSN: 2775-0833
https://jurnalequivalent.id/index.php/jequi/index
DOI: doi.org/10.59261/jequi.v8i4.445

Performance and Emission Analysis of Natural Gas–Hydrogen and Natural Gas–Ammonia Co-Firing in Aeroderevative Gas Turbines

Muhamad Falah Ramadhan*
Institut Teknologi Sepuluh November, Indonesia

Ary Bachtiar Krishna Putra
Institut Teknologi Sepuluh November, Indonesia

***Corresponding author:**
Muhamad Falah Ramadhan, Institut Teknologi Sepuluh November, Indonesia.
✉falahrmdn97@gmail.com

Article Info:

Article history:
Received: August 24, 2026
Revised: September 18, 2026
Accepted: October 5, 2026
Available Online: October 21, 2026

Keywords:
Aeroderivative Gas Turbine;
Tm2500+;
Cofiring;
Hydrogen;
Ammonia

This is an open access article under the CC BY-SA license.

Copyright © 2026 by Author. Published by Politeknik Siber Cerdika International

Abstract

Background: Increasing the use of hydrogen and ammonia as partial substitutes for natural gas through cofiring is one of the decarbonization strategies for the power generation sector in pursuit of net-zero emissions.
Objective: This study compares the effects of natural gas–hydrogen and natural gas–ammonia cofiring at volumetric blending ratios of 5–30% on the performance and emissions of a GE TM2500+ aeroderivative gas turbine at the Maleo gas-fired power plant (PLTG).
Methods: Thermodynamic cycle simulations were performed using Aspen HYSYS V14 at a constant volumetric fuel flow rate and a turbine inlet temperature of 1,230°C. Combustion kinetics were evaluated using ANSYS Chemkin-Pro with a reactor network comprising a perfectly stirred reactor, a gas mixer, and a plug flow reactor.
Results: Thermal efficiency increased under both cofiring scenarios. At a 30% cofiring ratio, natural gas–ammonia cofiring increased thermal efficiency from 37.05% to 37.44%, whereas natural gas–hydrogen cofiring increased it to 37.17%. Power turbine output decreased under both scenarios. Reductions in CO_2 mass flow rates were relatively comparable, whereas differences in CO_2 concentrations were primarily attributable to dilution effects. Hydrogen cofiring produced nonmonotonic NO_x emissions ranging from 23.4 to 25.5 ppm, whereas ammonia cofiring increased NO_x emissions to 2,987.6 ppm at a 30% cofiring ratio because of fuel-NO_x formation from fuel-bound nitrogen in ammonia.
Conclusion: Hydrogen cofiring offers a more balanced trade-off between efficiency and emissions within the investigated range, whereas ammonia cofiring requires additional NO_x mitigation measures before practical application at higher cofiring ratios.

To cite this article: Ramadhan, M. F., & Putra, A. B. K. (2026). Performance and emission analysis of natural gas–hydrogen and natural gas–ammonia co-firing in aeroderevative gas turbines. *Equivalent: Jurnal Ilmiah Sosial Teknik, 8*(4), 1852-1871. https://doi.org/10.59261/jequi.v8i4.445

INTRODUCTION

In the Indonesian context, the government's net-zero emissions (NZE) target for 2060 calls for significant decarbonization of the power sector. Natural gas-fired power plants (*Pembangkit Listrik Tenaga Gas*, PLTG), which currently provide critical baseload and peak-load generation capacity across Indonesia's archipelagic power networks, must transition to lower-carbon fuel pathways to support this national commitment while maintaining grid stability and operational reliability.

Global warming driven by increasing concentrations of greenhouse gases (GHGs) has become a major environmental threat in the 21st century. The 2015 Paris Agreement, adopted by 196 parties, reaffirmed the commitment to limit the increase in the global average temperature to well below 2°C above preindustrial levels while pursuing efforts to limit the increase to 1.5°C.

According to the *Emissions Gap Report 2025*, published by the United Nations Environment Programme (UNEP), global GHG emissions reached a record 57.7 gigatons of carbon dioxide equivalent ($GtCO_2e$) in 2024, representing an increase of approximately 3% compared with 2023 and 8% compared with the average for the preceding decade (2010–2019). Of this total, the power generation sector was the largest contributor, accounting for 15.6 $GtCO_2e$, or approximately 27% of total global emissions, followed by the transportation sector, at 8.4 $GtCO_2e$ (15%), and the energy industry, at 6.5 $GtCO_2e$ (11%) (United Nations Environment Programme, 2025).

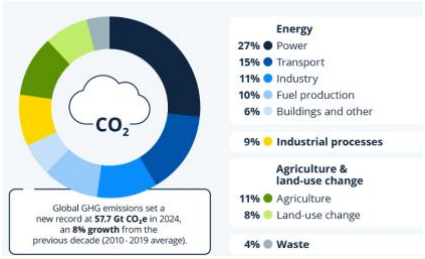


Figure 1. Total Greenhouse Gas Emissions in 2024 (United Nations Environment Programme, 2025)

Natural gas–fired gas power plants (*Pembangkit Listrik Tenaga Gas*, PLTG), although producing lower CO_2 emissions than coal-fired power plants, still contribute substantially to greenhouse gas emissions. The Cilegon PLTG, equipped with a Mitsubishi M701F gas turbine, produces up to 1.9 million metric tons of CO_2 annually, with an emissions intensity of 0.67 kg CO_2/kWh, exceeding the global average of 0.52 kg CO_2/kWh (Nugraha et al., 2025), These figures highlight the need for a planned and systematic emissions mitigation strategy for all PLTG units operating in Indonesia, including the GE TM2500+ gas turbine, an aeroderivative gas turbine manufactured by General Electric (GE). This turbine is a two-shaft unit with a maximum power output of up to 34.6 MW and a thermal efficiency of 37%. It uses a single-annular combustor (SAC) and can operate on dual fuel (Rahman & Etminan, 2026; Silalahi, 2025; Skabelund et al., 2023),

Co-firing natural gas with hydrogen is one potential strategy for reducing gas turbine emissions. Hydrogen has a lower heating value (LHV) per unit mass approximately 2.76 times that of natural gas. Consequently, replacing a portion of natural gas with hydrogen on a volumetric basis has the potential to improve the gas turbine cycle's thermal efficiency. For the M701F turbine, the average increase in thermal efficiency was reported to be 0.32–0.37 percentage points for every 5-percentage-point increase in the hydrogen (H_2) volume fraction in the fuel mixture Nugraha et al., (2025), Grigore et al. (2026) also reported an increase in thermal efficiency from 34.1% to 36.6% with 20 vol% H_2 co-firing in the Solar Titan 130 turbine. Similarly, Amrouche et al. (2025) reported a 2.9-percentage-point increase in thermal efficiency with 60 vol% H_2 co-firing in the GE MS5002C turbine. The main challenges associated with hydrogen co-firing include increased nitrogen oxide (NO_x) emissions due to potentially higher adiabatic flame temperatures and the risk of flashback in premixed combustion chambers because hydrogen has a substantially higher laminar flame speed than natural gas (Alikulov et al., 2024; Nugraha et al., 2025),

Co-firing natural gas with ammonia is another potential strategy because ammonia (NH_3) is a carbon-free fuel. Its idealized combustion with oxygen produces nitrogen (N_2) and water vapor (H_2O), according to the overall reaction $4NH_3 + 3O_2 \rightarrow 2N_2 + 6H_2O$ + heat (Zhang et al., 2025), Ammonia also benefits from relatively mature production, storage, and distribution infrastructure established through its industrial production, particularly the Haber–Bosch process. Nevertheless, natural gas–ammonia co-firing presents two fundamental technical challenges. First, ammonia has a laminar flame speed approximately one-fifth that of methane (CH_4), potentially resulting in flame instability under certain operating conditions (Zhang et al., 2025), Second, the nitrogen contained in NH_3 can contribute to NO_x formation through fuel-bound nitrogen pathways. Experimental findings have indicated that NO_x emissions from ammonia combustion can exceed those from pure CH_4 combustion by more than two orders of magnitude under specific conditions (Mengqing et al., 2025). Amrouche et al. (2025) , in a study involving a 7.6 MW gas turbine, reported that co-firing with 30% NH_3 produced NO_x emissions of 1,819.9 ppm at 15% O_2, substantially exceeding the applicable regulatory limit. In comparison, co-firing with

30% H_2 produced only 3.1 ppm NO_x.

Comparing these two co-firing scenarios is important because they present fundamentally different performance characteristics and technical challenges. Natural gas–hydrogen co-firing can improve thermal efficiency and may reduce certain emissions, but its environmental benefits depend on the hydrogen production pathway, and its implementation requires specialized hydrogen storage and distribution infrastructure. In contrast, natural gas–ammonia co-firing can benefit from more established fuel logistics and may reduce direct CO_2 emissions from combustion, depending on the substitution ratio and operating conditions; however, controlling NO_x emissions remains a major challenge. This study aims to analyze and compare the effects of the two co-firing scenarios at volumetric blending ratios of 5–30% on thermal efficiency and exhaust gas emissions in the GE TM2500+ aeroderivative gas turbine. Specifically, it addresses four research questions: (1) How do variations in the co-firing ratio affect thermal efficiency and power output from the power turbine in each scenario? (2) How do variations in the co-firing ratio affect turbine operating parameters? (3) Which alternative fuel provides better thermodynamic performance over the same blending-ratio range? and (4) How do the emissions produced by the two co-firing scenarios compare? Thermodynamic cycle analysis was performed using Aspen HYSYS, while combustion and emission characteristics were analyzed using ANSYS Chemkin-Pro. The objective was to develop a comprehensive understanding of thermal efficiency, CO_2 reduction, and NO_x emissions under both co-firing scenarios and to identify the most suitable co-firing strategy for the GE TM2500+ aeroderivative gas turbine in the context of Indonesia's energy transition toward net-zero emissions (NZE) by 2060.

This study was limited to the GE TM2500+ aeroderivative gas turbine operating at maximum load. Unit performance test data collected during nighttime operation were used as the basis for model validation because the compressor inlet air temperature significantly affects gas turbine performance. The volumetric fuel-blending ratios investigated were 0% (baseline), 5%, 10%, 15%, 20%, 25%, and 30%. Thermodynamic simulations were performed at a constant turbine inlet temperature (TIT) and constant volumetric fuel flow rate using the Peng–Robinson equation of state in Aspen HYSYS. Combustion kinetics simulations were conducted in ANSYS Chemkin-Pro using a perfectly stirred reactor (PSR) and a plug-flow reactor (PFR), together with the GRI-Mech 3.0 reaction mechanism. This study does not include three-dimensional computational fluid dynamics (CFD) analysis, fire or flashback dynamics, or techno-economic analysis.

METHOD

Research Objects and Unit Operation Data

The research object was the GE TM2500+ aeroderivative gas turbine, a two-shaft gas turbine manufactured by General Electric (GE) and developed from the LM2500+ aircraft engine technology. The unit was widely used in Indonesia as a mobile gas turbine power plant. The main technical specifications of the GE TM2500+ used as references for this study are presented in Table 1.

Table 1

Technical Specifications of GE TM2500+ Gas Turbine (Moliere & Lech, 2023)

Parameters	Values / Descriptions
Gas Turbine Type	Aeroderivative, Twin-shaft
Maximum Power Capacity	Up to 34.6 MW
Design Thermal Efficiency	37% (LM2500+ base)
High Pressure Compressor (HPC)	17 stages
High Pressure Turbine (HPT)	2 Stages
Power Turbine (PT)	6 stages
Combustion Room Type	Single Annular Combustor (SAC)
Combustion Type	Diffusion Combustion
Fuel Capability	Dual Fuel (Gas & Liquid)

Operational data used to validate the numerical models in Aspen HYSYS and ANSYS Chemkin-Pro were obtained during performance testing of the Maleo gas turbine power plant (*Pembangkit Listrik Tenaga Gas*, PLTG). The natural gas composition was based on gas chromatograph test results that had been validated against PLN operational logs, as presented in Table 2.

Table 2
Natural Gas Composition of Maleo Power Plant Chromatograph Gas Test Results

Composition	Mole Faction
Methane	0,9537
Ethane	0,0346
Propane	0,0078
i-Butane	0,0016
n-butane	0,0020
i-Pentane	0,0002
n-Pentane	0,0000
n-hexane	0,0000
Nitrogen	0,0001
Oxygen	0,0000
Carbon Dioxide	0,0000
LHV (BTU/scf)	953,0

The unit performance test data obtained at 100% load were used to validate the baseline model. These data covered the thermodynamic conditions at six key measurement points in the gas turbine cycle, as presented in Table 3.

Table 3
Maleo PLTG Unit Performance Test Data at 100% Load (Validation Basis)

Tags	Measurement Point	Parameters	Value
1	HPC IN	T (°C)	28,00
		P (kPa)	101,00
		Flow Mass (kg/h)	298.500,07
2	HPC OUT	T (°C)	497,00
		P (kPa)	2.084,00
6	GAS IN	T (°C)	29,00
		P (kPa)	2.334,00
		Flow Mass (kg/h)	4.747,00
		Flow Volume (m^3/h)	6.618,00
3	HPT IN	T (°C)	1.229,12
4	HPT OUT	T (°C)	818,00
		P (kPa)	430,40
5	PT OUT	T (°C)	538,92
		P (kPa)	101,00
		Power (kW)	24.300,00
		LHV (BTU/scf)	953,00
		Efficiency (%)	37,15

Research Simulation Scenarios

The natural gas–hydrogen (NG–H_2) and natural gas–ammonia (NG–NH_3) co-firing ratios were varied across 0%, 5%, 10%, 15%, 20%, 25%, and 30% of the total fuel mixture by volume. The upper limit of 30 vol% was selected based on recommendations attributed to Mitsubishi Heavy Industries and relevant literature. Ammonia co-firing ratios above 30% may require modifications to the combustion system because of challenges associated with NO_x emissions and combustion stability

under fuel-rich and fuel-lean conditions (Amrouche et al., 2025), The simulation scenarios are summarized in Table 4.

Table 4
GE TM2500+ Gas Turbine Cofiring Research Simulation Scenario

Parameters	Baseline (0%)	Scenario A (GA–H2)	Scenario B (GA–NH3)
Primary Fuel	Natural Gas	Natural Gas	Natural Gas
Secondary Fuel	–	Hydrogen (H2)	Ammonia (NH3)
Mixed Variations (vol.%)	0 (reference)	5,10,15,20,25,30	5,10,15,20,25,30
TIT Conditions	Constant 1.230°C	Constant 1.230°C	Constant 1.230°C
Simulation Tools	Aspen HYSYS	Aspen HYSYS + Chemkin-Pro	Aspen HYSYS + Chemkin-Pro

Cycle Thermodynamic Modeling with Aspen HYSYS V14

Model development in Aspen HYSYS began with the definition of a component list containing 14 chemical species: methane, ethane, propane, i-butane, n-butane, and i-pentane to represent natural gas; oxygen and nitrogen to represent combustion air; CO_2, CO, and H_2O as major combustion products; hydrogen and ammonia as co-firing fuels; and NO_2 and NO as nitrogen oxide species for emissions tracking. The Basis-1 fluid package was configured using the Peng–Robinson equation of state, consistent with Silalahi (2025) justification that this property model provides reliable predictions over a wide range of operating conditions for hydrocarbon and natural gas systems.

The combustion reactions were defined using an equilibrium-type reaction set associated with Basis-1. The set comprised eight individual reactions involving methane, ethane, n-butane, i-butane, propane, i-pentane, hydrogen, and ammonia. The stoichiometric equation for methane combustion was defined as follows:

$$CH4 + 2O2 \rightarrow CO2 + 2H2O$$

Similar stoichiometric equations were applied to the other hydrocarbons. The hydrogen combustion reaction was defined as:

$$2H2 + O2 \rightarrow 2H2O$$

The ammonia combustion reaction was defined according to the overall stoichiometric equation commonly used in Aspen HYSYS-based gas turbine co-firing studies:

$$4NH3 + 3O2 \rightarrow 2N2 + 6H2O$$

This reaction was consistent with the ammonia combustion approach applied by Amrouche et al. (2025) in their Aspen HYSYS modeling of natural gas–ammonia co-firing scenarios in combined heat and power systems.

The baseline process flow diagram (PFD) consisted of an HPC compressor that compressed the inlet air from 28°C and 101 kPa to the HPC outlet conditions, approximately 497–504°C and 2,084 kPa. A single-annular combustor (SAC), represented by an equilibrium reactor, modeled the conversion of the chemical energy of the fuel into thermal energy. The expansion system consisted of an HPT that drove the HPC through a common shaft and a power turbine (PT) that expanded the working fluid toward atmospheric pressure. Two flow dividers were also included to represent the distribution of air for cooling upstream of the HPT and the bypass air supplied upstream of the PT. An Adjust block (ADJ-1) iteratively regulated the inlet airflow rate to maintain a constant turbine inlet temperature (TIT) of 1,230°C for each simulated co-firing ratio. The co-firing models were developed from the baseline PFD by adding a secondary fuel stream hydrogen in Scenario A or ammonia in Scenario B and mixing it with the natural gas in an additional mixer before the mixture entered the SAC (Figures 2 and 3). In Scenario B, the ammonia stream was first passed through a heater to vaporize the ammonia and bring it to the specified inlet temperature of 55.57°C and pressure of 2,332 kPa, because the combustion reaction set was configured for the vapor phase (VaporPhase).

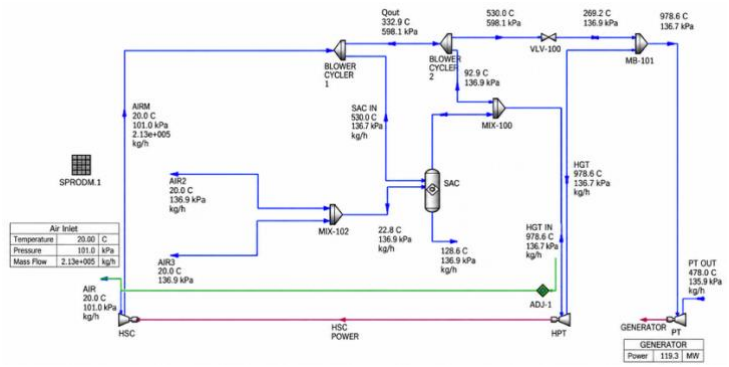


Figure 2. Process Flow Diagram of GE TM2500+ Gas Turbine in Natural Gas–Hydrogen Cofiring

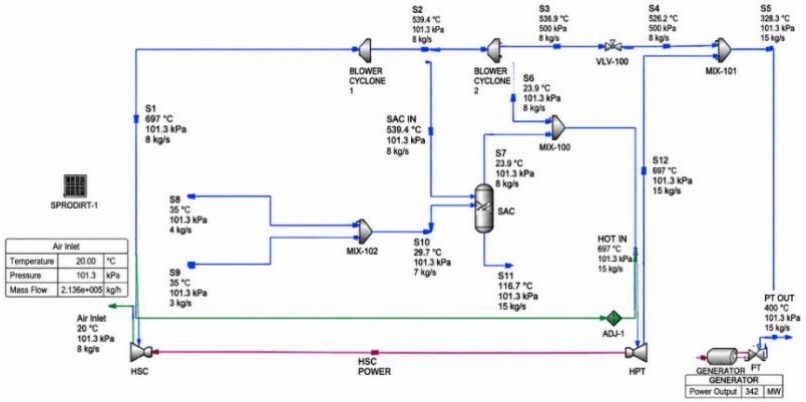


Figure 3. Process Flow Diagram of GE TM2500+ Gas Turbine in Cofiring Natural Gas–Ammonia

The inlet airflow was specified at 28°C and 101 kPa, with a mass flow rate of (2.776 \times 10^5) kg/h, based on the design data from the heat balance diagram in combination with the actual unit commissioning data. The natural gas stream was specified at 29°C and 2,334 kPa, with the molar composition given in Table 2 and an LHV of 49,705 kJ/kg. For the co-firing models, the flow rate of each fuel component was calculated according to the specified volumetric co-firing ratio (5–30%), while the total volumetric fuel flow rate was maintained at a constant value. The lower heating value of the fuel mixture ((LHV_{\mathrm{mix}})) was calculated using the volumetric mixing approach:

$$LHVmix = [(1 - CFR) \times LHVNG] + [CFR \times LHVH2 \text{ or } NH3]$$

where (CFR) denotes the volumetric fraction of the secondary fuel in the total fuel mixture. The component volumetric flow rates were subsequently converted to mass flow rates using the density of each gas under the specified reference conditions.

Combustion Kinetics Modeling with ANSYS Chemkin-Pro

After the Brayton-cycle thermodynamic model had been validated using Aspen HYSYS V14, combustion chemical kinetics modeling was performed using ANSYS Chemkin-Pro to obtain more detailed predictions of exhaust gas composition, including CO_2, CO, and NO_x, than those available from the chemical equilibrium approach in Aspen HYSYS. The chemical reactor network (CRN) consisted of a perfectly stirred reactor (PSR), representing the primary combustion zone; a gas mixer, representing the mixing of secondary air with the primary combustion products; and a plug-flow reactor (PFR), representing the downstream reaction zone. This two-zone combustion representation reflected the division of primary and secondary airflow in the HYSYS model, including the flow divider used to represent the distribution of cooling and bypass air, thereby maintaining structural consistency between the thermodynamic and combustion models. The NG–H_2 (Scenario A) and NG–NH_3 (Scenario B) co-firing models were developed from the baseline model by introducing a secondary fuel stream into the PSR alongside natural gas at volumetric co-firing ratios of 5–30%, representing the specified fuel-blending conditions (Figure 4).

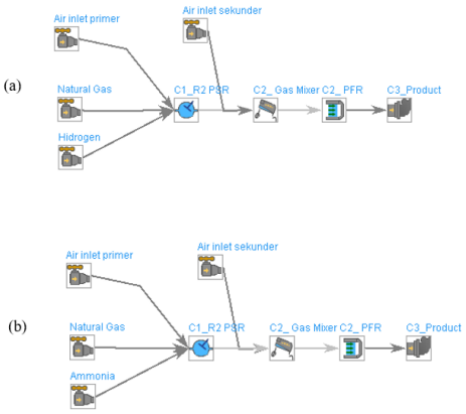


Figure 4. Diagram of the Chemical Reactor Network (CRN) of the Aeroderivative Gas Turbine TM2500+ on (a) Cofiring Natural Gas–Hydrogen and (b) Cofiring Natural Gas–Ammonia

Although GRI-Mech 3.0 has recognized limitations in representing ammonia combustion chemistry, it was selected for this study for three reasons: (1) its established validation history for natural gas and hydrogen combustion; (2) its computational efficiency for zero-dimensional (0D) reactor modeling; and (3) its relevance to the operating conditions of the Maleo power plant. Cross-validation against specialized ammonia combustion mechanisms (Okafor et al., 2024; Stagni et al., 2020) was recommended for future investigations of detailed reaction pathways.

The chemical mechanism used in this study was GRI-Mech 3.0, which contains five elements (C, H, O, N, and Ar), 53 chemical species, and 325 reactions. This mechanism was also used by Amrouche et al. (2025) in their performance and emissions analysis of ammonia–hydrogen fuel mixtures. The fuel and combustion air inputs in Chemkin-Pro were not specified independently; instead, they were obtained directly from the validated Aspen HYSYS simulations to maintain consistency in the thermodynamic operating conditions between the two software packages. The operating parameters obtained from the HYSYS simulations and subsequently used as inputs to Chemkin-Pro for Scenarios A and B are presented in Tables 5 and 6, respectively.

Table 5
Chemkin-Pro Simulation Input Parameters on Natural Gas–Hydrogen Cofiring Ratio Variation

Parameters	Units	0%	5%	10%	15%	20%	25%	30%
Flow mass air primer (SAC IN)	kg/s	37,01	35,67	34,34	33,00	31,67	30,34	29,00
Secondary air mass flow (2-2)	kg/s	32,32	31,15	29,98	28,82	27,65	26,49	25,32
Flow mass mixed fuel	kg/s	1,32	1,26	1,20	1,14	1,09	1,03	0,97
Flow mass natural gas	kg/s	1,32	1,25	1,19	1,12	1,05	0,99	0,92
Flow mass hydrogen	kg/s	0,000	0,008	0,016	0,024	0,031	0,039	0,047
Primary/secondary air temperature	°C	504	504	504	504	504	504	504
Natural gas & hydrogen temperature	°C	29	29	29	29	29	29	29
Pressure SAC IN (PSR)	kPa	2.084	2.084	2.084	2.084	2.084	2.084	2.084

Table 6
Chemkin-Pro Simulation Input Parameters on Natural Gas–Ammonia Cofiring Ratio Variations

Parameters	Units	0%	5%	10%	15%	20%	25%	30%
Flow mass air primer (SAC IN)	kg/s	37,01	35,78	34,56	33,33	32,09	30,90	29,67
Secondary air mass flow (2-2)	kg/s	32,32	31,24	30,18	29,11	28,02	26,98	25,91
Flow mass mixed fuel	kg/s	1,3185	1,32	1,32	1,32	1,32	1,32	1,32
Flow mass natural gas	kg/s	1,32	1,25	1,19	1,12	1,05	0,99	0,92
Flow mass ammonia	kg/s	0,000	0,067	0,134	0,201	0,269	0,333	0,401
Primary/secondary air temperature	°C	504	504	504	504	504	504	504

Parameters	Units	0%	5%	10%	15%	20%	25%	30%
Natural gas & ammonia temperature	°C	29	29	29	29	29	29	29
Pressure SAC IN (PSR-PFR)	kPa	2.084	2.084	2.084	2.084	2.084	2.084	2.084

The PSR was operated at 2,084 kPa, corresponding to the compressor discharge pressure, with a residence time of 3 ms based on the typical operating parameters of industrial gas turbines (Li & Li, 2021; Zhang et al., 2025), The gas mixer represented the rapid mixing of secondary air with the PSR outlet products without additional chemical reactions, with a mixing time of 1 ms. The PFR diameter was calibrated within a range of 60–70 cm to achieve a target residence time of 13–17 ms. Consequently, the total residence time of the system (PSR + mixer + PFR) was 17–20 ms, consistent with the residence-time parameters reported in CRN studies of heavy-duty gas turbines by Zhang et al. (2025) and Li & Li (2021). Each co-firing ratio was simulated in a separate project file, with the Continuation feature disabled. This approach was adopted because the PSR operated near the turning point of the ignition S-curve, where carrying over solutions between cases could introduce variations in NO_x predictions that did not reflect genuine physical trends. The output species extracted from the PFR at each fuel-blending ratio included CO_2, CO, and NO_x.

Emission Calculation Method

The simulated exhaust species concentrations could not be directly compared across cases or with emissions standards because the raw mole fractions were influenced by water vapor content (wet basis) and differences in excess oxygen concentrations under different operating conditions. Emissions were therefore calculated in four stages. First, the wet-basis mole fractions ((X_{i,\mathrm{wet}})) were extracted from the PFR output in Chemkin-Pro and the PT OUT stream in Aspen HYSYS. Second, the wet-basis mole fractions were converted to dry-basis values using the following equation:

$$X_{i,dry} = X_{i,wet} / (1 - X_{H2O,wet})$$

Third, the dry-basis mole fractions were converted to volumetric concentrations in parts per million (ppm):

$$C_i\ (ppm) = X_{i,dry} \times 10^6$$

Fourth, the concentrations were corrected to a reference oxygen concentration of 15% (O_2ref), following the approach applied by Silalahi (2025) to the same research object and consistent with established gas turbine emissions reporting practices. The correction was calculated as follows:

$$C_{corrected} = C_{measured,dry} \times (20.9 - O_{2,ref}) / (20.9 - O_{2,measured,dry})$$

where Ccorrected is the corrected emissions concentration (ppm, dry basis, at a reference oxygen concentration of 15%); Cdry is the measured dry-basis concentration; O2ref is the reference oxygen concentration (15%); and O2dry is the measured dry-basis oxygen concentration. The value of 20.9% represents the oxygen concentration in ambient air used in the correction formula.

RESULTS AND DISCUSSION

Model Validation

Before implementing the co-firing simulations, the basic model of the GE TM2500+ aeroderivative gas turbine developed in Aspen HYSYS V14 was validated by comparing the simulation results with the performance test data for the Maleo PLTG unit at 100% load. The comparison results are presented in Table 7.

Table 7
Simulation Model Validation Results on Unit Performance Data

Tags	Dot	Parameters	Test Data	Simulation	Error (%)
1	HPC IN	T (°C)	28,00	28,00	0,00
		P (kPa)	101,00	101,00	0,00
		Flow mass (kg/h)	298.500	277.500	7,04

Tags	Dot	Parameters	Test Data	Simulation	Error (%)
2	HPC OUT	T (°C)	497,00	504,10	1,43
		P (kPa)	2.084,00	2.084,00	0,00
6	GAS IN	T (°C)	29,00	29,00	0,00
		P (kPa)	2.334,00	2.334,00	0,00
		Flow mass (kg/h)	4.747,00	4.747,00	0,00
		Flow volume (m^3/h)	6.618,00	6.618,00	0,00
3	HPT IN	T (°C)	1.229,12	1.230,00	0,07
4	HPT OUT	T (°C)	818,00	788,60	3,59
		P (kPa)	430,40	430,60	0,05
5	PT OUT	T (°C)	538,92	499,00	7,41
		P (kPa)	101,00	101,00	0,00
		Power (kW)	24.300,00	24.300,00	0,00
		LHV (BTU/scf)	953,00	953,00	0,00
		Efficiency (%)	37,15	37,05	0,27

The percentage error for all parameters is below the 10% threshold. This criterion is consistent with the approach described by Cui et al. (2021) and Cui et al. (2024) , who stated that gas turbine thermodynamic simulations may be considered valid when the deviation from experimental or operational data does not exceed 10%. Thus, the basic model is considered sufficiently valid for use as the basis for developing the co-firing models in the subsequent stages.

Effect of Cofiring on Fuel Characteristics of Blends

This subsection evaluates changes in fuel blend characteristics resulting from the co-firing of natural gas–hydrogen (Scenario A) and natural gas–ammonia (Scenario B) at volumetric blending ratios of 0–30%, while maintaining a constant total fuel volumetric flow rate of 6,618 m^3/h, consistent with the existing fuel metering system of the Maleo PLTG unit.

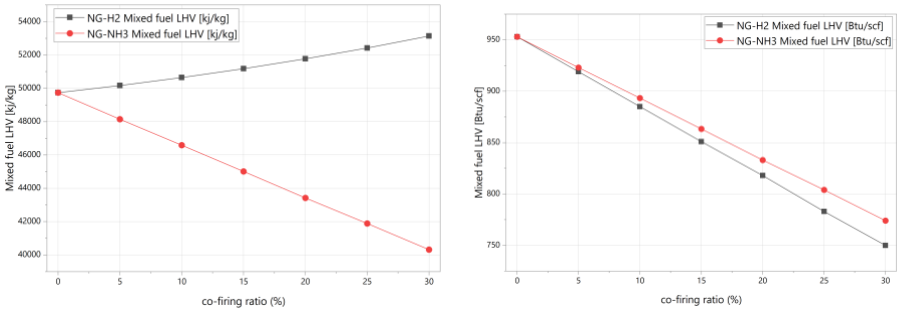


Figure 5. Effect of Cofiring Ratio on Volumetric Base LHV (left) and Mass Base LHV (right)

The volumetric-basis LHV decreases in both scenarios as the co-firing ratio increases. In Scenario A, the volumetric-basis LHV decreases from 953 Btu/scf at a 0% hydrogen blending ratio to 750 Btu/scf at a 30% hydrogen blending ratio, representing a decrease of 21.30%. In Scenario B, it decreases to 774 Btu/scf at a 30% ammonia blending ratio, representing a decrease of 18.78%. This decrease results from the lower volumetric energy density of hydrogen and ammonia compared with natural gas. At ambient pressure, the volumetric energy density of natural gas can be approximately 3.5 times that of hydrogen (Habib et al., 2024), The volumetric-basis LHV values across the investigated co-firing ratios (750–953 Btu/scf) remain above the stated minimum TM2500+ fuel-flexibility limit of 650 Btu/scf. Therefore, both scenarios satisfy this particular fuel-heating-value constraint, although overall operational feasibility also depends on other fuel specifications and combustor operating limits.

On a mass basis, the two scenarios exhibit opposite trends. In Scenario A, the mass-basis LHV increases from 49,740 to 53,140 kJ/kg at a 30% hydrogen blending ratio, representing an increase of 6.84%. In Scenario B, it decreases to 40,320 kJ/kg at the same blending ratio, representing a decrease of 18.94%. This difference can be explained by the gravimetric heating values of the

individual fuels. Hydrogen has a mass-basis LHV of approximately 119.9 MJ/kg, or about 2.4 times that of methane. Consequently, increasing the hydrogen fraction raises the LHV per unit mass of the blend. Conversely, ammonia has a substantially lower mass-basis LHV, thereby reducing the LHV per unit mass as its fraction increases. As reported by Silalahi (2025) , an increase in the mass-basis LHV of the fuel blend contributes to changes in the Back Work Ratio (BWR) and turbine outlet temperature (TOT) through changes in the energy available to drive the high-pressure turbine (HPT) and the resulting compressor work. This relationship may help explain the differences in BWR and thermal-efficiency trends between the two scenarios discussed in Section 3.4.

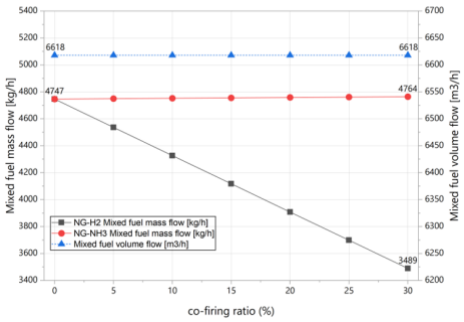


Figure 6. Effect of Cofiring Ratio on Fuel Flow Mass

The most pronounced difference between the two scenarios is observed in the mass flow rate of the fuel blend. In Scenario A, the mass flow rate decreases from 4,747 to 3,489 kg/h at a 30% hydrogen blending ratio, representing a decrease of 26.50%. In Scenario B, the mass flow rate remains nearly constant, increasing slightly from 4,747 to 4,764 kg/h, or approximately 0.36%. This difference can be explained by the densities of the respective gases. Hydrogen has a much lower density (approximately 0.09 kg/m^3) than natural gas (approximately 0.72 kg/m^3). Therefore, at a constant total volumetric flow rate, replacing natural gas with hydrogen substantially reduces the total mass of the fuel blend. In contrast, the density of ammonia (approximately 0.73 kg/m^3) is close to that of natural gas, so replacing natural gas with ammonia has only a marginal effect on the total fuel mass flow rate. These findings help explain the differences in thermal-efficiency behavior between the two scenarios discussed in the following subsection.

Effect of Cofiring on Turbine Operational Parameters

In both scenarios, compressor work decreases monotonically and approximately linearly as the co-firing ratio increases. The baseline compressor work is identical in both scenarios at 39.00 MW. At a 30% blending ratio, compressor work reaches 30.56 MW in Scenario A and 31.27 MW in Scenario B, a difference of 0.71 MW. Overall, compressor work decreases by 8.44 MW (21.64%) in Scenario A and by 7.73 MW (19.82%) in Scenario B.

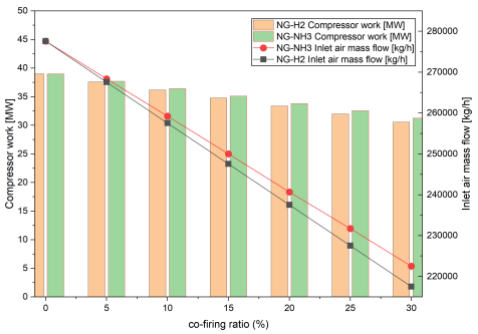


Figure 7. The Effect of Cofiring Ratio on Compressor and Turbine Work

The PSR reactor represents the primary combustion zone within the SAC. Its outlet temperature is an important indicator of combustion conditions in the primary zone and provides an initial condition for assessing NO_x formation in the subsequent plug-flow reactor (PFR). Under

baseline conditions, both scenarios produce an identical PSR temperature of 1,746.48°C. As the co-firing ratio increases, the PSR temperature decreases gradually in Scenario A, reaching 1,744.56°C at a 30% hydrogen blending ratio, a decrease of 1.92°C. In Scenario B, the temperature decreases more substantially, reaching 1,736.71°C at a 30% ammonia blending ratio, a decrease of 9.77°C approximately five times the decrease observed in Scenario A. This difference can be partly explained by the thermochemical properties of the two fuels. Hydrogen can support higher adiabatic flame temperatures than methane under certain combustion conditions; Habib et al. (2024) , for example, reported values of 2,207°C for hydrogen and 1,941°C for methane at 1 atm. Accordingly, hydrogen addition may help maintain flame temperature, consistent with the findings of Amrouche et al. (2025), In contrast, ammonia has a much lower laminar burning velocity than methane, approximately one-fifth under the conditions cited, and its endothermic thermal dissociation ($NH_3 \rightarrow ½N_2 + 3/2H_2$) can absorb heat, potentially contributing to a lower flame temperature. The magnitude of these effects, however, depends on the combustion conditions and the assumptions used in the model.

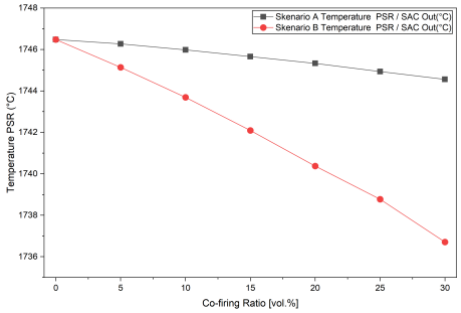


Figure 8. Effect of Cofiring Ratio on PSR/SAC Temperature

The turbine outlet temperature (TOT, corresponding to the HPT outlet temperature in the model) was evaluated to assess operational feasibility against the stated maximum limit of 855°C and minimum limit of 204.4°C (Aminaho et al., 2025; Freitag et al., 2024; Silalahi, 2025), Although the turbine inlet temperature (TIT) was maintained at approximately 1,230°C, the TOT increased monotonically in both scenarios. In Scenario A, the TOT increases from 788.4°C to 789.2°C at a 30% hydrogen blending ratio, representing an increase of approximately 0.10%. In Scenario B, it increases to 793.0°C, representing an increase of approximately 0.58%. This behavior can be interpreted through the turbine energy balance, expressed approximately as TOT = TIT − ΔT_HPT, where ΔT_HPT is the temperature drop across the HPT. The temperature drop depends on the extracted turbine work and the effective heat capacity of the working gas, in Table 8.

Table 8
Temperature Difference Change of HPT Expansion (Δ T_HPT) at 0% and 30% Ratio

Scenario	Δ T_HPT (0%)	Δ T_HPT (30%)	Changes
Scenario A	441.6°C	440.8°C	−0.8°C (−0.18%)
Scenario B	441.6°C	437.0°C	−4.6°C (−1.04%)

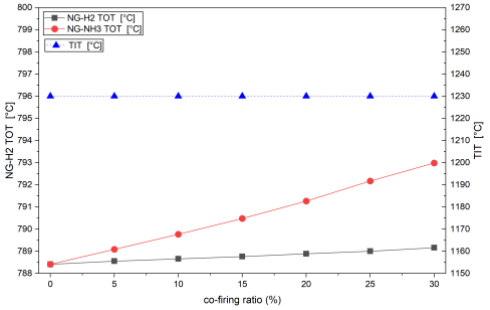


Figure 9. The Effect of Cofiring Ratio on Turbine Outlet Temperature (TOT)

The temperature drop across the HPT decreases in both scenarios, with a substantially greater decrease in Scenario B than in Scenario A. This pattern is consistent with the larger increase in TOT and the greater decrease in BWR observed in Scenario B. The agreement among these trends supports the internal consistency of the simulation results. The increase in TOT is associated with the decrease in ΔT_HPT and changes in the working gas's thermodynamic properties. However, the precise contributions of gas composition, mass flow rate, heat capacity, and turbine work should be established from the model's energy and mass balances rather than attributed solely to changes in water vapor content. In particular, hydrogen and ammonia combustion both produce water vapor, but the resulting temperature change also depends on the fuel–air ratio, combustion products, and turbine operating conditions.

The residence time in the PFR increases monotonically in both scenarios as the co-firing ratio increases, as shown in Table 9. In Scenario A, residence time increases from 16.723 ms at baseline to 21.323 ms at a 30% hydrogen blending ratio, representing an increase of 27.51%. In Scenario B, it increases to 20.786 ms at a 30% ammonia blending ratio, representing an increase of 24.30%.

Table 9
Residence Time PFR in Both Cofiring Scenarios

Cofiring Ratio [vol.%]	Scenario A: Residence Time PFR (ms)	Scenario B: Residence Time PFR (ms)
0	16,723	16,723
5	17,366	17,325
10	17,811	17,887
15	18,736	18,556
20	19,370	19,276
25	20,361	19,962
30	21,323	20,786

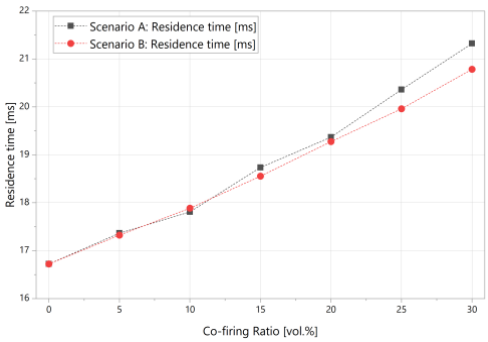


Figure 10. The Effect of Cofiring Ratio on Residence Time PFR

The increase in residence time in both scenarios can be interpreted using the fundamental relationship for a flow reactor, τPFR = VPFR/Q̇total, where τPFR is the residence time, VPFR is the reactor volume, and Q̇total is the total volumetric flow rate through the reactor. Because the PFR volume is fixed, residence time is inversely proportional to the total volumetric flow rate. If the total volumetric flow rate decreases as the combustion-air flow rate decreases, residence time will increase accordingly. The reported reductions in air mass flow rate in both scenarios (21.65% in Scenario A and 19.85% in Scenario B at a 30% blending ratio) may therefore contribute to the longer PFR residence times. However, this interpretation should be verified using the actual volumetric flow rates at the PFR conditions, since mass flow rate and volumetric flow rate are not interchangeable when gas composition, temperature, and pressure vary. The residence-time trends cross between the 5% and 10% blending ratios, after which Scenario A consistently exhibits a longer residence time than Scenario B. The difference reaches 0.537 ms at a 30% blending ratio, consistent with the greater reported reduction in airflow in Scenario A. Longer residence times can provide more time for chemical reactions, including the Zeldovich reaction ($N_2 + O \rightleftharpoons NO + N$), which underlies thermal NO_x formation. Because this reaction is temperature-sensitive and involves endothermic reaction steps,

changes in residence time and temperature can influence the NO_x emission characteristics discussed in Section 3.5.

Effect of Cofiring on Thermal Efficiency, Turbine Power and Back Work Ratio

The Aspen HYSYS V14 simulation results, obtained at a constant TIT of approximately 1,230°C and a constant total fuel volumetric flow rate, show changes in three principal performance parameters: Power Turbine (PT) output power, cycle thermal efficiency (η), and Back Work Ratio (BWR). These changes reflect the control strategy of the existing fuel metering system at the Maleo PLTG unit (Božo et al., 2019; Jeong et al., 2024), The simulation results are summarized in Table 10.

Table 10
PT Power Recapitulation, Thermal Efficiency, and Back Work Ratio in Both Cofiring Scenarios

Cofiring Ratio [vol.%]	Power PT A (MW)	Efficiency A (%)	BWR A	Power PT B (MW)	Efficiency B (%)	BWR B
0	24,3014	37,0542	0,6161	24,3014	37,0542	0,6161
5	23,4404	37,0745	0,6159	23,5763	37,1121	0,6152
10	22,5791	37,0899	0,6157	22,8594	37,1662	0,6144
15	21,7215	37,1055	0,6155	22,1339	37,2263	0,6134
20	20,8602	37,1205	0,6153	21,4000	37,2848	0,6124
25	20,0025	37,1411	0,6151	20,7002	37,3637	0,6113
30	19,1439	37,1683	0,6148	19,9742	37,4333	0,6101

PT output power decreases monotonically in both scenarios. In Scenario A, PT output power decreases from 24.3014 MW to 19.1439 MW at a 30% hydrogen blending ratio, representing a decrease of 21.22%. In Scenario B, the decrease is smaller, from 24.3014 MW to 19.9742 MW, representing a decrease of 17.80%. This decrease is associated with the constant-volume fuel-flow control strategy. Because the co-firing ratio is defined on a volumetric rather than an energy basis, partially replacing natural gas with H_2 or NH_3 at a constant total volumetric flow rate reduces the volumetric-basis LHV of the blend and, consequently, the chemical energy supplied to the combustion chamber. This mechanism is consistent with the findings of Silalahi (2025) for the same TM2500+ unit, which reported a reduction in PT output power of up to 29.5% at 100% hydrogen co-firing. The difference in the magnitude of the decrease between the two scenarios can be explained in part by differences in fuel density and volumetric LHV. L. Mustafa et al. (2025) reported densities of approximately 0.66, 0.08, and 0.73 kg/m^3 for CH_4, H_2, and NH_3, respectively, under the standard conditions used in their study, together with volumetric LHVs of 33.4, 9.6, and 13.7 MJ/m^3, respectively. Although hydrogen has a much higher mass-basis LHV than ammonia (119.9 versus 18.8 MJ/kg; Habib et al. (2024) , its much lower density results in a lower energy content per unit volume. Consequently, the volumetric energy deficit in Scenario B is smaller than that in Scenario A.

In contrast to the PT power trends, cycle thermal efficiency increases monotonically in both scenarios. In Scenario A, efficiency increases from 37.0542% to 37.1683% at a 30% hydrogen blending ratio, an increase of 0.114 percentage points. In Scenario B, efficiency increases more substantially, reaching 37.4333%, an increase of 0.379 percentage points. The increase in efficiency despite the decrease in output power is consistent with studies of hydrogen and ammonia co-firing under constant-TIT strategies. Silalahi (2025) reported a 1.12% increase in efficiency at 100% hydrogen co-firing in TM2500+ units, attributing the improvement to a reduction in BWR. Mendoza Morales et al. (2024) reported a 2.26% increase in cycle efficiency in 25–35 MW-class aeroderivative turbines operating with hydrogen under a constant-TIT strategy. Grigore et al. (2026) , studying a Solar Titan 130 turbine operating with an 80/20 vol. % CH_4/H_2 mixture, reported an increase in efficiency from 34.1% to 36.6%. The greater efficiency increase in Scenario B is also consistent with the findings of L. Mustafa et al. (2025) for the GE LM6000 turbine, which indicated that increasing the ammonia proportion in a CH_4/NH_3 blend can improve thermal efficiency under the modeled operating conditions.

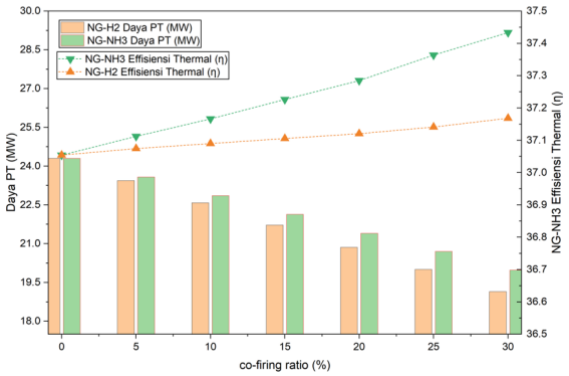


Figure 11. The Effect of Cofiring Ratio on Thermal Efficiency and Turbine Power

The BWR, defined here as the ratio of compressor work to the combined output of the HPT and PT (BWR = WHPC/(WHPT + WPT)), decreases monotonically in both scenarios. In Scenario A, BWR decreases from 0.6161 to 0.6148 at a 30% hydrogen blending ratio, a decrease of approximately 0.21%. In Scenario B, BWR decreases more substantially, reaching 0.6101, a decrease of approximately 0.97%. The decrease in BWR indicates that the fraction of the combined turbine work required to drive the compressor becomes smaller as the co-firing ratio increases, leaving a relatively larger fraction available as net output. These findings are consistent with Silalahi (2025) , who reported a decrease in BWR from 0.610 to 0.596 at 100% hydrogen co-firing in the same TM2500+ unit.

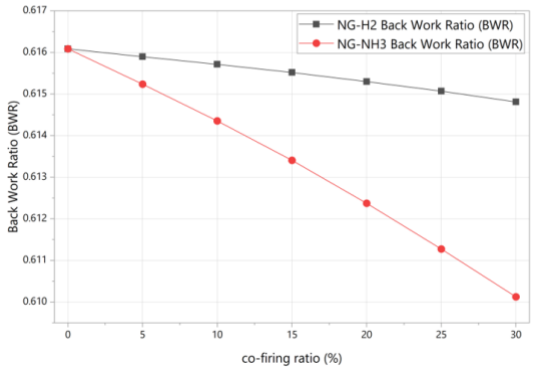


Figure 12. The Effect of Cofiring Ratio on Back Work Ratio (BWR)

Overall, the simulation results reveal a consistent trade-off in both scenarios: the decrease in PT output power is accompanied by an increase in cycle thermal efficiency and a decrease in BWR. At the same co-firing ratio, Scenario B consistently exhibits a smaller reduction in power output, a larger increase in efficiency, and a greater decrease in BWR than Scenario A. These differences can be partly explained by the higher volumetric energy density of NH_3 compared with H_2 (K. F. Mustafa & Slefarski, 2024), These efficiency improvements must be considered alongside the reduction in net output power, which is an inherent trade-off associated with the constant-volume control strategy modeled after the existing fuel metering system at the Maleo power plant.

Exhaust Emission Characteristics

Carbon Dioxide (CO2) Emissions

The simulated CO_2 concentrations at the PFR outlet exhibit a monotonically decreasing trend in both scenarios. At a 30% co-firing ratio, the concentration decreases from a baseline of 3.332% to 2.957% in Scenario A and 2.865% in Scenario B, corresponding to decreases of 11.26% and 14.02%, respectively. This decrease can be attributed to two simultaneous mechanisms. First, replacing natural gas with hydrogen or ammonia reduces the carbon content of the fuel blend because both hydrogen and ammonia are carbon-free fuels. Consequently, fewer carbon atoms are available for oxidation to CO_2. Second, the addition of combustion products that do not contain carbon dilutes the CO_2 concentration. In Scenario B, ammonia combustion produces additional N_2

through the oxidation of hydrogen and the subsequent formation of water, as represented by the overall reaction $NH_3 + 0.75O_2 \rightarrow 0.5N_2 + 1.5H_2O$. This additional N_2 increases the total exhaust-gas molar flow and can contribute to a greater reduction in CO_2 concentration than in Scenario A. The combined effects help explain why the CO_2 concentration decreases more sharply in Scenario B. However, the absolute CO_2 mass flow rates must be evaluated separately because concentration reductions do not necessarily correspond to equivalent reductions in mass emissions. Any claim that the mass flow rates are approximately equivalent should be verified against the simulated exhaust-gas flow rates and carbon balances.

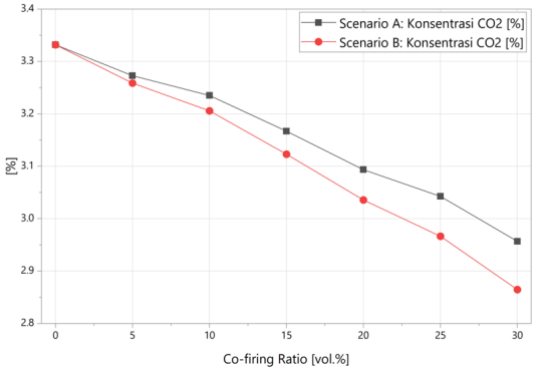


Figure 13. The Effect of Cofiring Ratio on CO2 Emissions

Nitrogen Oxide (NOx) emissions

NO_x emissions were analyzed using ANSYS Chemkin-Pro simulation data at the PFR outlet, which represents the modeled exhaust-gas conditions of the gas turbine. The results reveal substantial differences between Scenario A and Scenario B in both the emission trends and the underlying formation mechanisms, as presented in Table 11.

Table 11
NO, NO2, and NOx Emission Concentrations in Both Cofiring Scenarios

Cofiring Ratio [vol.%]	NO A (ppm)	NO2 A (ppm)	NOx A (ppm)	NO B (ppm)	NO2 B (ppm)	NOx B (ppm)
0	24,79	0,475	25,260	24,79	0,475	25,26
5	24,13	0,464	24,591	971,18	18,778	989,96
10	25,54	0,486	26,027	1.544,97	29,686	1.574,66
15	24,81	0,477	25,290	1.992,31	38,632	2.030,94
20	23,40	0,455	23,853	2.372,89	46,259	2.419,15
25	24,96	0,479	25,441	2.688,30	52,098	2.740,39
30	24,15	0,467	24,620	2.987,59	58,340	3.045,93

In Scenario A, the simulation results show nonmonotonic, sawtooth-like fluctuations in NO concentrations, which range from 23.40 to 25.54 ppm. The mean concentration is approximately 24.54 ppm, with a coefficient of variation of 2.64%, rather than the expected monotonically increasing trend. A simple linear regression of the NO data yields a slope of approximately −0.017 ppm per percentage-point increase in the H_2 blending ratio. This slope is small relative to the observed fluctuations and does not establish a meaningful systematic trend. Within the investigated range of 0–30%, the effect of hydrogen addition on NO_x formation may therefore be difficult to distinguish from numerical variability or the sensitivity of the modeled thermal-NO_x mechanism, commonly associated with the extended Zeldovich mechanism, to small changes in PSR temperature. This result differs from that of Silalahi (2025) , who reported a 41.22% increase in NO at a 100% hydrogen blending ratio. The difference does not necessarily indicate a contradiction, because the studies examined different co-firing ranges and may have used different modeling assumptions and operating conditions. The NO_2/NO_x ratio in Scenario A remains relatively stable at approximately 1.868–1.908% across the investigated co-firing ratios, with a mean of approximately 1.887%. This stability suggests that the modeled conversion of NO

to NO_2 through reactions such as NO + HO_2 → NO_2 + OH remains relatively consistent under the simulated conditions.

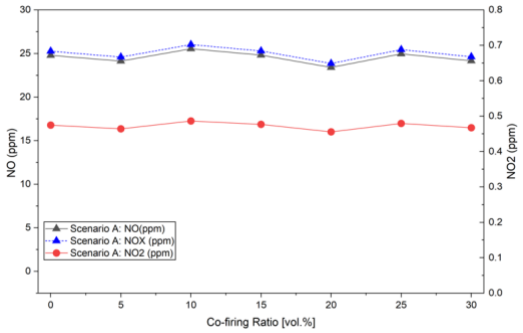


Figure 14. Effect of Cofiring Ratio on NO and NO2 Emissions in Scenario A

The nonmonotonic sawtooth pattern in Scenario A, with NO_x concentrations ranging from approximately 23.4 to 25.5 ppm, may reflect several factors: (1) numerical sensitivity or convergence behavior in the PSR at low NO_x concentrations; and (2) competing effects associated with changes in flame temperature and combustion chemistry as hydrogen is added. The fluctuations alone, however, are insufficient to establish that solver convergence is the cause. Further testing of numerical tolerances, solver convergence criteria, reaction-mechanism sensitivity, and repeatability would be needed to distinguish numerical artifacts from genuine chemical responses. Adjusting the convergence tolerances in Chemkin-Pro and conducting a sensitivity analysis could help clarify the origin of these fluctuations in future simulations.

Scenario B exhibits markedly different behavior. The NO concentration increases monotonically from 24.79 ppm at baseline to 2,987.59 ppm at a 30% ammonia blending ratio, an increase of approximately 120-fold. The incremental increases become progressively smaller with each additional 5 percentage points of ammonia. Unlike Scenario A, in which thermal NO_x is expected to be a major formation pathway, the sharp increase in Scenario B is consistent with the influence of fuel-bound nitrogen introduced by NH_3. Ammonia can undergo sequential dehydrogenation through reactions involving H radicals, including NH_3 + H → NH_2 + H_2, NH_2 + H → NH + H_2, and NH + H → N + H_2. The resulting nitrogen-containing intermediates can participate in pathways that form NO, including reactions involving NH_2 and O to produce HNO, followed by reactions that convert HNO to NO. Competing pathways can also reduce NO, for example through reactions involving NH_2 and NO that produce N_2 and H_2O. The resulting NO_x concentration reflects the competition among these formation and reduction pathways.

A quantitative comparison using a 15% O_2 reference correction yielded a corrected NO_x concentration of approximately 2,664.6 ppm at a 30% ammonia blending ratio. This result is of the same order of magnitude as the value of 1,819.9 ppm at 15% O_2 reported by Amrouche et al. (2025) for 30% NH_3 co-firing in a 7.6 MW gas turbine using a similar modeling approach. The values differ by a factor of approximately 1.46, potentially reflecting differences in combustor design, turbine capacity, operating conditions, chemical mechanisms, and model assumptions. The oxygen-reference correction and the comparability of the reported concentrations should be verified against the original sources. A technical review by Mitsubishi Heavy Industries, as cited by Amrouche et al. (2025) , recommends limiting the ammonia fraction to approximately 30 vol. % to avoid the need for excessive combustor enlargement associated with high NO_x emissions. The simulated NO_x concentrations, which reach thousands of ppm at a 30% ammonia blending ratio, underscore the importance of NO_x mitigation when evaluating ammonia co-firing.

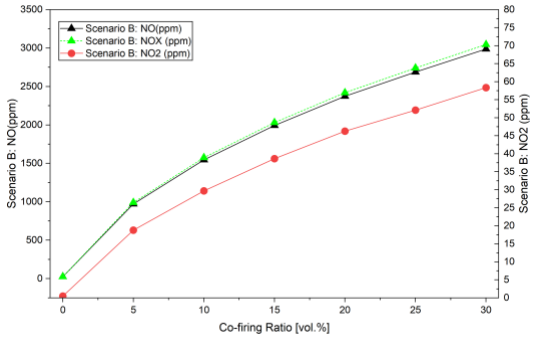


Figure 15. Effect of Cofiring Ratio on NO and NO2 Emissions in Scenario B

Comparative Synthesis of NOx Emissions of the Second Scenario

Table 12
Quantitative Comparison of the Two Scenarios at a Cofiring Ratio of 30%

Parameters	Scenario A (30% H2)	Scenario B (30% NH3)	B/A Ratio
NO (ppm)	24,15	2.987,59	123,7
NO2 (ppm)	0,467	58,340	125,0
Total NOx (ppm)	24,62	3.045,93	123,7
Trend form	Sawtooth (noise-dominated)	Monotonic, diminishing returns	–
Dominant mechanism	Thermal NOx (Zeldovich)	Fuel-NOx (HNO/NHi)	–

The approximately 124-fold difference in NO_x concentrations indicates that ammonia co-firing exhibits a fundamentally different NO_x formation profile from hydrogen co-firing, reflecting differences in the dominant chemical pathways rather than merely differences in magnitude. Nevertheless, the NO_2/NO_x ratios in both scenarios remain within a relatively narrow range of approximately 1.868–1.915%, despite the substantial difference in total NO_x concentrations. This similarity suggests that the modeled post-flame oxidation of NO to NO_2 may be relatively insensitive to the primary nitrogen source under the simulated conditions. However, the NO_2/NO_x ratio alone does not establish that the post-flame oxidation mechanism operates independently of the primary NO_x formation pathway. The conversion fraction may also depend on temperature, residence time, and the availability of HO_2, O_2, and other reactive species.

Discussion

The results presented in the preceding section collectively address the four research questions posed in the Introduction and support a consistent physical interpretation rather than four separate findings. The first two questions how the co-firing ratio affects thermal efficiency, PT output power, and other operating parameters can be interpreted through a common underlying mechanism. At constant TIT and constant total fuel volumetric flow rate, replacing natural gas with a secondary fuel of different density and volumetric LHV changes the fuel mass flow rate, fuel energy input, combustion-product composition, and potentially the airflow and compressor operating point. These changes influence the BWR and cycle thermal efficiency, even as PT output power decreases. Because hydrogen and ammonia have different densities and volumetric energy contents relative to natural gas, the modeled effects differ between the two scenarios. This helps explain why Scenario B exhibits a greater reduction in BWR, a larger efficiency increase, and a smaller reduction in PT output power at every investigated blending ratio. These relationships should nevertheless be interpreted in light of the model's control strategy and assumptions about compressor and turbine operation.

The third and fourth research questions which fuel performs better thermodynamically and how the emissions compare do not yield a single overall winner. This is a central finding of

the study. When evaluated solely in terms of modeled thermal efficiency and BWR, ammonia co-firing performs better at every investigated ratio. When evaluated in terms of NO_x formation, however, the two fuels produce markedly different results: hydrogen co-firing remains within a narrow range of modeled NO_x concentrations, whereas ammonia co-firing exhibits a substantial, monotonic increase toward concentrations that would likely require additional emissions-control measures before practical deployment. This asymmetry is consistent with the different dominant chemical pathways identified in Section 3.5. Thermal NO_x formation through the Zeldovich mechanism is strongly temperature-dependent, while fuel-NO_x formation is influenced by the nitrogen introduced into the flame through ammonia. Thus, even a fuel that offers thermodynamic advantages may be constrained by emissions before its efficiency benefits can be fully realized.

For the Maleo PLTG unit and comparable GE TM2500+ installations operating within Indonesia's net-zero-emissions-by-2060 (NZE 2060) roadmap, this trade-off has direct practical implications. Hydrogen co-firing provides a modest modeled efficiency gain of approximately 0.11 percentage points at a 30% blending ratio, while the predicted NO_x concentrations remain close to the baseline values. This suggests that hydrogen co-firing could be a promising near-term option for the existing single-annular combustor, subject to validation of combustion stability, material compatibility, emissions performance, hydrogen availability, and fuel cost. Ammonia co-firing offers a larger modeled efficiency gain and may benefit from established production and logistics infrastructure associated with the Haber–Bosch process. However, the NO_x concentration predicted in this study approximately 2,988 ppm at 30% ammonia, or approximately 2,665 ppm after correction to 15% O_2 would likely exceed applicable emissions limits if representative of actual stack emissions. Consequently, realizing ammonia's efficiency advantage would likely require effective NO_x mitigation, such as staged combustion, selective catalytic reduction (SCR), or another suitable emissions-control strategy. Hydrogen co-firing is therefore recommended as the more balanced near-term option under the conditions investigated. This recommendation reflects its potentially lower emissions-control burden within the modeled range, rather than a conclusion that ammonia is thermodynamically inferior.

Several limitations constrain the generalizability of these conclusions. First, the Aspen HYSYS cycle model uses an equilibrium Reaction Set rather than finite-rate chemical kinetics. Although this approach can support the evaluation of overall energy and mass balances, it cannot independently resolve combustion stability, flashback risk, or blow-off. These phenomena are particularly relevant because hydrogen has a high laminar flame speed, whereas ammonia has a comparatively low flame speed, and they were explicitly excluded from the scope of this study. Second, the Chemkin-Pro PSR–Mixer–PFR network, although structurally aligned with the thermodynamic model, relies on GRI-Mech 3.0, a mechanism developed primarily for natural gas and hydrocarbon combustion. Its predictions for ammonia-related nitrogen chemistry may therefore be more uncertain than those obtained using mechanisms specifically validated for NH_3/H_2 combustion. This limitation could contribute to differences between the corrected NO_x concentration obtained in this study and the value reported by Amrouche et al. (2025) for a different turbine and combustor. Third, model validation was performed at a single operating point corresponding to 100% load during nighttime operation. Consequently, part-load behavior, which is relevant to a mobile PLTG installation such as the Maleo unit, remains untested. Finally, the investigated co-firing range of 0–30%, selected with reference to the Mitsubishi Heavy Industries recommendation cited in the literature, leaves the NO_x behavior of ammonia co-firing beyond 30% and the long-term economics of both fuel pathways unresolved. These limitations also inform the directions for further research discussed below.

CONCLUSION

Based on the Aspen HYSYS and ANSYS Chemkin-Pro simulations, natural gas–hydrogen co-firing (Scenario A) and natural gas–ammonia co-firing (Scenario B) at volumetric blending ratios of 0–30% both increased the modeled thermal efficiency of the GE TM2500+ aeroderivative gas turbine. Scenario B produced a greater efficiency increase, from 37.05% to 37.44%, compared with Scenario A, which increased from 37.05% to 37.17%. However, PT output power decreased in both scenarios under the constant total fuel volumetric flow-rate control strategy, with reductions of 21.22% in Scenario A and 17.80% in Scenario B. The reductions in CO_2 mass flow

rate were reported to be relatively similar between the two scenarios, whereas the difference in the percentage reduction in CO_2 concentration was primarily associated with dilution by nitrogen-containing combustion products in Scenario B. This interpretation should be confirmed through a comparison of the simulated exhaust-gas flow rates and carbon balances. The most pronounced difference was observed in NO_x emissions: Scenario A produced nonmonotonic NO_x concentrations of approximately 23.4–25.5 ppm, whereas Scenario B exhibited a sharp increase to approximately 2,987.6 ppm at a 30% ammonia blending ratio, consistent with the influence of fuel-bound nitrogen on NO_x formation.

Considering the trade-off between thermal efficiency and exhaust emissions, hydrogen co-firing appears to offer a more balanced option within the investigated 0–30% blending range. In contrast, ammonia co-firing would require additional NO_x mitigation technologies, such as staged combustion or selective catalytic reduction (SCR), particularly at higher blending ratios. Further research should validate ammonia-related fuel-NO_x chemistry using a reaction mechanism specifically suited to NH_3 combustion rather than relying solely on GRI-Mech 3.0, investigate ammonia co-firing ratios above 30% to characterize the NO_x response, and conduct techno-economic assessments of domestic ammonia supply and the investment requirements associated with NO_x mitigation technologies.

ACKNOWLEDGEMENT

The authors would like to express their appreciation to all parties who provided academic and technical support during the completion of this research. Their assistance contributed to the successful completion of the study.

AUTHOR CONTRIBUTION STATEMENT

Muhamad Falah Ramadhan: Conceptualization, methodology, simulation, data analysis, visualization, and writing original draft. Ary Bachtiar Krishna Putra: Conceptualization, methodology, supervision, validation, and research guidance. Both authors contributed to the interpretation of the research findings and approved the final manuscript for publication.

REFERENCES

Alikulov, K., Aminov, Z., Tran, V. T., Le, T. H., Nguyen, X. P., Dong, V. H., & Kim, W. (2024). Comparative analysis of 100% ammonia–hydrogen and cofiring with natural gas in 7.6 MW industrial gas turbine a comprehensive Aspen HYSYS study. *International Journal of Hydrogen Energy*, *89*, 332–348.

Aminaho, E. N., Aminaho, N. S., & Aminaho, F. (2025). Techno-economic assessments of electrolyzers for hydrogen production. *Applied Energy*, *399*. https://doi.org/10.1016/j.apenergy.2025.126515

Amrouche, F., Erickson, P. A., Varnhagen, S., & Park, J. W. (2025). Performance analysis of hydrogen co-firing in a GE MS-5002C heavy-duty gas turbine. *International Journal of Hydrogen Energy*, *102*, 458–471.

Božo, G., Valera-Medina, A., Syred, N., & Bowen, P. (2019). Fuel quality impact analysis for practical implementation of corn cob gasification gas in conventional gas turbine power plants. *Biomass and Bioenergy*. https://doi.org/10.1016/j.biombioe.2019.01.012

Cui, H. C., Lai, X. T., Wu, J. F., Wang, M. Z., Liu, W., & Liu, Z. C. (2021). Overall numerical simulation and experimental study of a hybrid oblique-rib and submerged jet impingement/microchannel heat sink. *International Journal of Heat and Mass Transfer*, *167*, 120839.

Cui, H. C., Zhang, Z. K., Yu, M. J., Liu, Z. C., & Liu, W. (2024). A hybrid slot jet impingement/microchannel heat sink for cooling high-power electronic devices: A combined experimental and numerical study. *International Journal of Thermal Sciences*, *197*. https://doi.org/10.1016/j.ijthermalsci.2023.108823

Freitag, P., Stolle, D., Kullmann, F., Linssen, J., & Stolten, D. (2024). A techno-economic analysis of future hydrogen reconversion technologies. *International Journal of Hydrogen Energy*, *77*. https://doi.org/10.1016/j.ijhydene.2024.06.164

Grigore, R., Hazi, A., Hazi, G., & Vernica, S. G. (2026). Influence of hydrogen cofiring with natural gas on thermal performance of a Solar Titan 130 gas turbine. *Energies*, *18*(4), 956.

Habib, M. A., Abdulrahman, G. A. Q., Alquaity, A. B. S., & Qasem, N. A. A. (2024). Hydrogen combustion, production, and applications: a review. *Alexandria Engineering Journal*, *100*, 182–207.

Jeong, J. H., Park, H. S., Park, Y. K., & Kim, T. S. (2024). Analysis of the influence of hydrogen co-firing on the operation and performance of the gas turbine and combined cycle. *Case Studies in Thermal Engineering*, *54*, 104061.

Li, S., & Li, S. (2021). Effects of hydrogen addition on the NOx emissions of NH3 combustion in a rich-lean staged combustor. *International Journal of Hydrogen Energy*, *46*(79), 39580–39592.

Mendoza Morales, M. M., Camacho Tauta, J. F., & Cardenas Garcia, D. (2024). Hydrogen cofiring effects on power output and thermal efficiency of an aeroderivative CHP gas turbine. *Energies*, *17*(14), 3433.

Mengqing, L., Yituan, H., Yuhao, W., & Shiyong, L. (2025). Effects of methane addition on combustion characteristics of ammonia-air co-flow flames. *Energy*, *335*, 138007. https://doi.org/10.1016/j.energy.2025.138007

Moliere, M., & Lech, A. (2023). Aeroderivative vs heavy-duty gas turbines for power generation: a comparative review. *Journal of the Global Power and Propulsion Society*, *7*, 250–267.

Mustafa, K. F., & Slefarski, R. (2024). NOx emission characteristics of hydrogen-enriched methane combustion in industrial gas turbines: a review. *International Journal of Hydrogen Energy*, *76*, 314–331.

Mustafa, L., Ślefarski, R., Jankowski, R., Alnajideen, M., & Eckart, S. (2025). Modeling the thermodynamics of oxygen-enriched combustion in a GE LM6000 gas turbine using CH4/NH3 and CH4/H2. *Energies*, *18*(12), 3221. https://doi.org/10.3390/en18123221

Nugraha, M. G., Sundari, R., Sasongko, D., Kurnia, K. A., & Indarto, A. (2025). Impact of hydrogen cofiring with natural gas on thermal efficiency and CO2 emissions of M701F gas turbine power plant. *International Journal of Hydrogen Energy*, *105*, 145–158.

Rahman, M. S., & Etminan, A. (2026). Techno-economic assessment and gas turbine integration of green hydrogen for power generation in Canada. *International Journal of Hydrogen Energy*, *227*. https://doi.org/10.1016/j.ijhydene.2026.154458

Silalahi, R. N. (2025). *Thermodynamic and techno-economic analysis of hydrogen cofiring in aeroderivative gas turbines*.

Skabelund, B. B., Jenkins, C. D., Stechel, E. B., & Milcarek, R. J. (2023). Thermodynamic and emission analysis of a hydrogen/methane fueled gas turbine. *Energy Conversion and Management: X*, *19*. https://doi.org/10.1016/j.ecmx.2023.100394

United Nations Environment Programme. (2025). *Emissions Gap Report 2025: Off Target*. United Nations Environment Programme. https://www.unep.org/en/publications/report/emissions-gap-report-2025

Zhang, M., An, Z., Wei, X., Wang, J., Huang, Z., & Tan, H. (2025). Emission characteristics and reaction mechanisms of ammonia combustion: a comprehensive review. *Renewable and Sustainable Energy Reviews*, *208*, 115041.